The relation of cosmic environment and morphology with the star formation and stellar populations of AGN and non-AGN galaxies

G. Mountrichas[1], G. Yang[2,3], V. Buat[4,5], B. Darvish[6], M. Boquien[7], Q. Ni[8], D. Burgarella[4] and L. Ciesla[4]

[1] Instituto de Fisica de Cantabria (CSIC-Universidad de Cantabria), Avenida de los Castros, 39005 Santander, Spain e-mail: `gmountrichas@gmail.com`
[2] Kapteyn Astronomical Institute, University of Groningen, P.O. Box 800, 9700 AV Groningen, The Netherlands
[3] SRON Netherlands Institute for Space Research, Postbus 800, 9700 AV Groningen, The Netherlands
[4] Aix Marseille Univ, CNRS, CNES, LAM Marseille, France.
[5] Institut Universitaire de France (IUF)
[6] University of California, Riverside, 900 University Avenue, Riverside, CA 92521, USA
[7] Centro de Astronomía (CITEVA), Universidad de Antofagasta, Avenida Angamos 601, Antofagasta, Chile
[8] Max-Planck-Institut für extraterrestrische Physik (MPE), Gießenbachstraße 1, D-85748 Garching bei München, Germany

June 7, 2023

ABSTRACT

In this work, we study the relation of cosmic environment and morphology with the star-formation (SF) and the stellar population of galaxies. Most importantly, we examine if this relation differs for systems with active and non-active supermassive black holes. For that purpose, we use 551 X-ray detected active galactic nuclei (AGN) and 16,917 non-AGN galaxies in the COSMOS-Legacy survey, for which the surface-density field measurements are available. The sources lie at redshift of $0.3 < z < 1.2$, probe X-ray luminosities of $42 < \log [L_{X,2-10keV}(\mathrm{erg\,s^{-1}})] < 44$ and have stellar masses, $10.5 < \log [M_*(M_\odot)] < 11.5$. Our results show that isolated AGN (field) have lower SFR compared to non AGN, at all L_X spanned by our sample. However, in denser environments (filaments, clusters), moderate L_X AGN ($\log [L_{X,2-10keV}(\mathrm{erg\,s^{-1}})] > 43$) and non-AGN galaxies have similar SFR. We, also, examine the stellar populations and the morphology of the sources in different cosmic fields. For the same morphological type, non-AGN galaxies tend to have older stellar populations and are less likely to have undergone a recent burst in denser environments compared to their field counterparts. The differences in the stellar populations with the density field are, mainly, driven by quiescent systems. Moreover, low L_X AGN present negligible variations of their stellar populations, in all cosmic environments, whereas moderate L_X AGN have, on average, younger stellar populations and are more likely to have undergone a recent burst, in high density fields. Finally, in the case of non-AGN galaxies, the fraction of bulge-dominated (BD) systems increases with the density field, while BD AGN are scarce in denser environments. Our results are consistent with a scenario in which a common mechanism, such as mergers, triggers both the SF and the AGN activity.

1. Introduction

It is widely accepted that galaxies and the supermassive black hole (SMBHs) in their centres co-evolve. This symbiosis has been demonstrated in a variety of ways. For instance, tight correlations have been found between the black hole mass and various galaxy properties (e.g., bulge or stellar mass, stellar velocity dispersion; Magorrian et al. 1998; Ferrarese & Merritt 2000; Tremaine et al. 2002; Kormendy & Ho 2013). Moreover, both the SMBH activity and star formation peak at similar cosmic times (z ∼ 2; e.g., Boyle et al. 2000; Sobral et al. 2013). In addition, both the black hole and galaxy growth are fed by cold gas.

A popular method to examine the co-evolution of galaxies and SMBHs is to study the relation between the star-formation rate (SFR) of the galaxy and the accreting power of the SMBH in their centre. For the latter, the X-ray luminosity, L_X, is used as a proxy in galaxies that host active SMBHs. These galaxies are known as active galactic nuclei (AGN). Although, this has been the topic of many studies (e.g. Lutz et al. 2010; Page et al. 2012; Lanzuisi et al. 2017), more information can be gained regarding the effect of the AGN feedback on the host galaxy, by comparing the SFR of AGN with that of non-AGN systems, with similar stellar mass, M_* and redshift (e.g. Rosario et al. 2013; Mullaney et al. 2015; Masoura et al. 2018; Bernhard et al. 2019; Florez

et al. 2020; Masoura et al. 2021; Koutoulidis et al. 2022; Pouliasis et al. 2022). Recent studies that applied this method found that for galaxies with $10.5 < \log [M_*(M_\odot)] < 11.5$ the SFR of low-to-moderate L_X ($42 < \log [L_{X,2-10keV}(\mathrm{erg\,s^{-1}})] < 44$) AGN tends to be lower, or at most equal to the SFR of non-AGN, star-forming galaxies, while an enhancement of ∼ 30% was found for the SFR of galaxies that host higher L_X AGN compared to non-AGN systems. Nevertheless, in both lower mass and more massive galaxies the SFR of AGN was similar to that of non-AGN systems (Mountrichas et al. 2021, 2022c,a). These results were also supported by studying the stellar populations of low-to-moderate L_X AGN compared to non-AGN systems (Mountrichas et al. 2022b).

A limitation of the above works is that they do not take into account the cosmic environment of the two populations (i.e., AGN and non-AGN systems). A significant number of studies, though, have investigated if and how the cosmic web affects the star-formation of galaxies (non-AGN), both in the local Universe and at high redshifts (e.g. Brambila et al. 2023; Song et al. 2023). At low redshifts (z < 1), most studies suggest that quiescent (Q) galaxies preferentially live in dense environments, such as groups and clusters, whereas star-forming galaxies are more commonly found in the field (e.g. Lin et al. 2014; Erfanianfar et al. 2016). A plausible scenario to interpret these results is that cold gas is removed in satellite galaxies due to their in-

teraction with the warm intra-cluster medium. At high redshifts, though, this picture seems to be either reversed (e.g., Elbaz et al. 2007; Santos et al. 2014) or no difference has been found in the SFR of galaxies that live in different density fields (e.g., Scoville et al. 2013; Cooke et al. 2023). Furthermore, a number of studies have shown that one of the galaxy properties that are mostly influenced by the cosmic environment is the galaxy morphology (e.g., Dressler 1980; Fasano et al. 2015). Nevertheless, these studies do not take into account the activity of the SMBH. In other words, they do not differentiate between AGN and non-AGN galaxies.

In this work, we compare the SFR and star-formation histories (SFH) of AGN and non-AGN systems, for different cosmic environments (field, filaments, clusters) and morphologies (bulge-dominated, BD, and non bulge-dominated, non-BD). Our goal is to examine the effect of AGN feedback on the host's star-formation in different density fields and compare the role of the cosmic web and morphology on the stellar population of AGN and non-AGN galaxies. For that purpose, we use sources detected in the COSMOS field and lie at z ∼ 1. We compute M_* by applying spectral energy distribution (SED) fitting using the CIGALE code, probing a range of $10.5 < \log[M_*(M_\odot)] < 11.5$. First, we compare the SFR of galaxies that host AGN with their non-AGN counterparts as a function of the cosmic environment. Then, we compare the effect of the density field and morphology on the stellar populations of AGN and non-AGN galaxies. Finally, we discuss our results and describe our main conclusions. Throughout this work, we assume a flat ΛCDM cosmology with $H_0 = 70.4\,\text{Km s}^{-1}\,\text{Mpc}^{-1}$ and $\Omega_M = 0.272$ (Komatsu et al. 2011).

2. Data

2.1. The X-ray dataset

In this study, we use sources that lie within the COSMOS field (Scoville et al. 2007). The X-ray AGN have been observed by the COSMOS-Legacy survey (Civano et al. 2016). This is a 4.6 Ms *Chandra* program that covers 2.2 deg² of the COSMOS region. The central area has been observed with an exposure time of ≈ 160 ks while the remaining area has an exposure time of ≈ 80 ks. The limiting depths are 2.2×10^{-16}, 1.5×10^{-15}, and 8.9×10^{-16} erg cm^{-2} s^{-1} in the soft (0.5-2 keV), hard (2-10 keV), and full (0.5-10 keV) bands, respectively. The X-ray catalogue includes 4016 sources. Marchesi et al. (2016) matched the X-ray sources with optical and infrared counterparts using the likelihood ratio technique (Sutherland & Saunders 1992). Of the sources, 97% have an optical and IR counterpart and a photometric redshift (photo-*z*) and ≈ 54% have spectroscopic redshift (spec-*z*). Photo-*z* have been derived from high-quality ultraviolet-to-infrared data (up to 32 bands; Laigle et al. 2016). Hardness ratios (HR = $\frac{H-S}{H+S}$, where H and S are the net counts of the sources in the hard and soft band, respectively) were estimated for all X-ray sources using the Bayesian estimation of hardness ratios method (BEHR; Park et al. 2006). The intrinsic column density, N_H, for each source was then calculated using its redshift and assuming an X-ray spectral power law with slope $\Gamma = 1.8$. This information is available in the catalogue presented in Marchesi et al. (2016). In this work, we use sources within the UltraVISTA region (1.38 deg² McCracken et al. 2012) of the COSMOS field. There are 1718 X-ray sources within this region with $\log[L_{X,2-10\text{keV}}(\text{erg s}^{-1})] > 42$.

In our analysis, we use the X-ray dataset used in Mountrichas et al. (2022c). Specifically, we use the same strict photomet-

ric selection criteria with them, to make sure that only sources with the best photometric coverage are included in our analysis (u, g, r, i, z, J, H, K_s, IRAC1, IRAC2, and MIPS/24, where IRAC1, IRAC2, and MIPS/24 are the [3.6] μm, [4.5] μm, and 24 μm photometric bands of Spitzer). We also apply the same reliability requirements with those described in Sect. 3.2 in Mountrichas et al. (2022c) to make certain that the analysis is restricted to those sources with the most reliable host galaxy properties (see Sect. 3). We, also, use only sources that meet the mass completeness limits, as described in detail in sections 2.1, 3.2 and 3.4 in Mountrichas et al. (2022c). Specifically, for the redshift range spanned by the sample, the stellar mass completeness limits are $\log[M_{*,95\%\text{lim}}(M_\odot)] = 9.13$ and 9.44 at $0.5 < z < 1.0$ and $1.0 < z < 1.5$, respectively. There are 1161 X-ray sources that meet all the above selection criteria (Table 2 in Mountrichas et al. 2022c).

One goal of this study is to examine the SFR of galaxies that host AGN in different cosmic environments. Yang et al. (2018), used sources in the COSMOS field, at $0.3 < z < 3.0$ and studied the dependence of the black hole growth on the cosmic environment. For that purpose, they adopted the 'weighted adaptive kernel smoothing' method to construct the surface-density field that probes sub-Mpc physical scales (Darvish et al. 2015). The method was applied to all sources in the COSMOS field, that is for both non-AGN galaxies and X-ray systems. The end product of this analysis is the calculation of the dimensionless overdensity parameter ($1 + \delta = \frac{\Sigma}{\Sigma_{median}}$, where Σ is the surface number density, in units of Mpc^{-2}, and Σ_{median} is the median Σ at each redshift). The method is described in detail in Sect. 2.3.1 in Yang et al. (2018) (see also Darvish et al. 2015). Based on the density field estimates, the cosmic-web is, then, extracted using the multiscale environment filter (MMF) algorithm (e.g., Aragón-Calvo et al. 2007; Darvish et al. 2014, 2017). The main idea is to measure the geometry of the density field around each point at each redshift. If the geometry is similar to that of a typical cluster or filament, then the point's environment is classified as cluster or filament. Otherwise, the point is classified as the field (for more details, see Sect. 2.3.2 in Yang et al. 2018).

To add to our X-ray sources the information about the field density and cosmic environment, we cross-match the 1161 sources with the catalogue used in Yang et al. (2018). This results in 1005 X-ray AGN. The missing AGN (1161 vs. 1005) are due to the fact that in Yang et al. (2018), they filter out sources near (< 1Ṁpc) the edge of the field, since density measurements for these sources are unreliable (see also Darvish et al. 2017).

2.2. The galaxy control sample

The main goal of this work, is to compare the SFR and SFH of AGN host galaxies in different cosmic environments with the SFR of non-AGN systems, in similar density fields. Towards this end, we use the galaxy control sample presented in Mountrichas et al. (2022c) (see their Sect. 2.2). We apply the same selection criteria used for the X-ray dataset and the same mass completeness limits, which result in 89375 sources (Table 2 in Mountrichas et al. 2022c). We note that X-ray sources have been excluded from the galaxy control sample, as well as sources with a strong AGN component, calculated by the SED fitting (see next section and Sect. 3.3 in Mountrichas et al. 2022c). To include information about the cosmic environment of the sources in the galaxy control sample, we cross-match it with the catalogue presented in Yang et al. (2018). There are 76,251 common sources between the two datasets.

3. Galaxy properties

In this section, we describe how we obtain information about the properties of the sources used in our analysis. Specifically, we present how we measure the SFR and M_* of AGN and non-AGN galaxies and how we retrieve knowledge on their stellar populations and morphology.

3.1. Calculation of SFR and M_*

The (host) galaxy properties of both the X-ray AGN and the galaxies in the control sample have been calculated via SED fitting, using the CIGALE code (Boquien et al. 2019; Yang et al. 2020, 2022). The SED fitting analysis is described in detail in Section 3.1 in Mountrichas et al. (2022c). In brief, the galaxy component is modelled using a delayed SFH model with a function form SFR $\propto$ t×exp($-$t/τ). A star formation burst is included (Ciesla et al. 2017; Małek et al. 2018; Buat et al. 2019) as a constant ongoing period of star formation of 50 Myr. Stellar emission is modelled using the single stellar population templates of Bruzual & Charlot (2003) and is attenuated following the Charlot & Fall (2000) attenuation law. To model the nebular emission, CIGALE adopts the nebular templates based on Inoue (2011). The emission of the dust heated by stars is modelled based on Dale et al. (2014), without any AGN contribution. The AGN emission is included using the SKIRTOR models of Stalevski et al. (2012, 2016). CIGALE has the ability to model the X-ray emission of galaxies. In the SED fitting process, the observed L_X in the $2 - 10$ keV band are used, provided by the Marchesi et al. (2016). The parameter space used is shown in Table 1 in Mountrichas et al. (2022c). The reliability of the SFR measurements, both in the case of AGN and non-AGN systems, has been examined in detail in our previous works and, in particular, in Sect. 3.2.2 in Mountrichas et al. (2022c).

In Mountrichas et al. (2021, 2022c,a), we found that the SFR_{norm}-L_X relation depends on the stellar mass range probed by the sources. Specifically a flat SFR_{norm}-L_X relation was found for the least and most massive systems ($\log[M_*(M_\odot)] < 10.5$ and $\log[M_*(M_\odot)] > 11.5$), with $SFR_{norm} \sim 1$. Albeit, for intermediate stellar masses ($10.5 < \log[M_*(M_\odot)] < 11.5$) SFR_{norm} was found to be $SFR_{norm} \leq 1$ at low-to-moderate L_X ($\log[L_{X,2-10keV}(\mathrm{erg\,s^{-1}})] < 44$) whereas at higher L_X, $SFR_{norm} > 1$ (e.g., see Fig. 5 in Mountrichas et al. 2022a). Among the 1005 X-ray AGN in our dataset, $\sim 80\%$ (809 sources) have $10.5 < \log[M_*(M_\odot)] < 11.5$. Therefore, there are not enough sources to probe lower or higher M_* in a statistically robust manner. Thus, we restrict our analysis to AGN (and galaxies) with $10.5 < \log[M_*(M_\odot)] < 11.5$. Furthermore, sources in our datasets (AGN and non-AGN) associated with filaments or the field, span redshifts up to 2.5. Nevertheless, in our samples, sources in clusters lie at $z < 1.2$. To make sure that our results and conclusions are not affected by the different redshift ranges probed by sources in different cosmic environments, we also restrict both our AGN and non-AGN datasets to $z < 1.2$. There are 551 (430 of which with spec-z) X-ray AGN and 16917 (6653 of which with spec-z) non-AGN galaxies that meet these two criteria (M_*, redshift). Among them, 31 (1048) AGN (non-AGN) are associated with clusters, 328 (9622) AGN (non-AGN) with filaments and 192 (6247) AGN (non-AGN) are in the field. The distribution of AGN in the L_X−redshift plane is presented in Fig. 1. These sources are used in the analysis presented in Sect. 4.1.
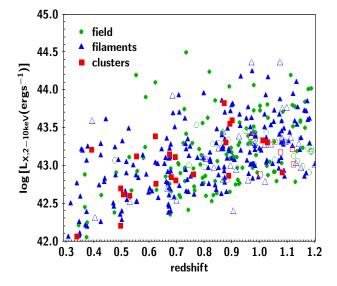

Fig. 1: The distribution of the 551 X-ray AGN in the L_X−redshift plane. Different colours and symbols correspond to sources associated with different cosmic environments, as indicated in the legend. Open symbols present AGN with photo-z.
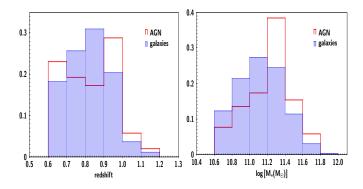

Fig. 2: Distributions of galaxy properties. The left panel shows the distributions of redshift and the right panel of M_*, for the 52 AGN (red histograms) and 1172 non-AGN galaxies (blue shaded histograms), used to study the SFH of the two populations.

3.2. Star-formation history

In Mountrichas et al. (2022b), we examined the SFH of AGN and non-AGN galaxies and we found that AGN of low-to-moderate L_X ($\log[L_{X,2-10keV}(\mathrm{erg\,s^{-1}})] < 44$) tend to have older stellar populations and are less likely to have experienced a recent star formation burst compared to non-AGN systems. Here, we study the SFH of the two populations, but, in addition, we take into account their cosmic environment (Sect. 4.2). For that purpose, we cross-match our AGN and galaxies in the control sample with the LEGA-C catalogue (van der Wel et al. 2016; Straatman et al. 2018; van der Wel et al. 2021). This catalogue includes spectra for 4081 galaxies (3741 unique objecs) within $0.6 < z < 1.3$. We make use of two stellar-age-sensitive tracers that are available in the LEGA-C dataset. These are the equivalent width (EW) of H_δ absorption, and the D_n4000 index (e.g., Kauffmann et al. 2003; Wu et al. 2018). D_n4000 is small for young stellar populations and large for old, metal-rich galaxies. On the other hand, the EW of H_δ rises rapidly in the first few hundred million years after a burst of star formation, when O- and B-type stars dominate the spectrum, and then decreases when A-type stars fade (e.g., Kauffmann et al. 2003; Wu et al. 2018).

We apply the same quality selection criteria described in Sect. 2.2.3 in Mountrichas et al. (2022b) that reduce the number of sources in the LEGA-C catalogue to 2834. Then, we cross match our X-ray and galaxy control samples with the LEGA-C dataset. This results in 52 AGN and 1,172 non-AGN galaxies. The average uncertainties on H_δ and D_n4000 are 17% and 3%, respectively. We note that the control sample has been reduced to those sources with $\log[M_*(M_\odot)] > 10.6$ to better match the M_* range of the X-ray dataset. The redshift and M_* distributions of the two populations are shown in Fig. 2. Both distributions are similar between the two populations. A Kolmogorov-Smirnov (KS) test gives a p-value of 0.57 and 0.12 for the redshift and M_* distributions of AGN and non-AGN galaxies, respectively (two distributions differ with a statistical significance of $\sim 2\sigma$ for a p-value of 0.05). Similar values are found applying a Mann-Whitney test (p-value of 0.90 and 0.29, respectively, for the redshift and M_* distributions). Therefore, we consider that the M_* and redshift distributions of AGN and non-AGN galaxies are not significantly different to affect the results presented in Sect. 4.2. Nevertheless, we confirm that if we account for the (small) differences in the redshift and M_* distributions of the two populations, following the methodology described in e.g., Mountrichas et al. (2019); Masoura et al. (2021); Buat et al. (2021); Mountrichas et al. (2022b) (i.e., weigh the sources based on their M_* and redshift), it does not change our results and overall conclusions.

3.3. Morphology

To examine the role of morphology of AGN and non-AGN galaxies in different cosmic environments (see Sect 4.3), we use the catalogue presented in Ni et al. (2021). The morphological classification was done using a deep-learning-based method to separate sources into BD and non-BD galaxies. The term BD refers to galaxies that only display a significant spheroidal component, without obvious disc-like or irregular components (for more information, see Appendix C and Sect. 2.3 in Ni et al. 2021; Yang et al. 2019, respectively).

We cross-match the datasets described in Sect. 3.2 with the catalogue of Ni et al. (2021), which results in 37 AGN and 1086 non-AGN galaxies. Type 1 AGN have been removed from the Ni et al. (2021) sample, since they can potentially affect host galaxy morphological measurements (see their Sect. 2.4). We also note, that the redshift and M_* distributions of AGN and non-AGN galaxies used in this part of our analysis, are very similar to those presented in Fig. 2 and thus we assume that the small differences in the redshift and M_* distributions of the two populations, do not affect our results.

4. Results

In this section, we compare the SFR of AGN and non-AGN galaxies as a function of the L_X, for different cosmic environments. We also examine if the results of this comparison are affected by the exclusion of quiescent systems from both populations. Furthermore, we study the SFH of the two population for different density fields. Finally, we compare the effect of morphology and environment on the stellar populations of AGN and non-AGN systems.

Fig. 3: SFR_{norm} ($= \frac{\text{SFR}_{\text{AGN}}}{\text{SFR}_{\text{non-AGN}}}$) as a function of L_X. Median values are presented. The measurements are grouped in bins of L_X, of 0.5 dex width. The errors presented are 1σ, calculated using bootstrap resampling. The top panel presents the results when we classify sources based on their cosmic environment, as indicated in the legend. The middle panel shows the results when sources are classified using their overdensity values (see text for more details). The bottom panel is similar to the top panel, but we have restricted our dataset to $0.8 \leq z \leq 1.2$.

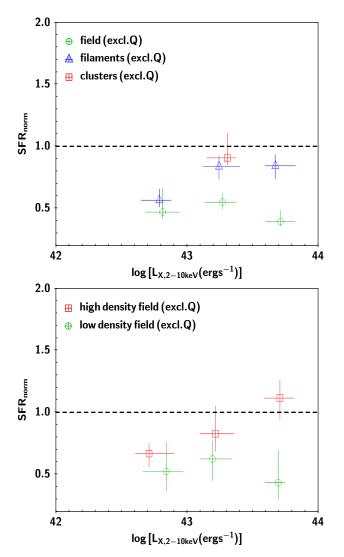Fig. 4: Same as Fig. 3, but excluding quiescent (Q) systems both from the AGN and galaxy samples.

4.1. Comparison of the SFR of AGN and non-AGN galaxies, as a function of L_X and cosmic environment

First, we compare the SFR of AGN host galaxies with the SFR of non-AGN systems, as a function of the cosmic environment. For that purpose, we use the SFR_{norm} parameter. SFR_{norm} is defined as the ratio of the SFR of galaxies that host AGN to the SFR of non-AGN systems, with similar M_* and redshift (e.g., Mullaney et al. 2015; Masoura et al. 2018; Bernhard et al. 2019; Masoura et al. 2021; Mountrichas et al. 2021, 2022c,a). For the estimation of SFR_{norm} we use the X-ray and galaxy control samples described in Sect. 2. SFR_{norm} is measured following the process of our previous studies (e.g., Mountrichas et al. 2021, 2022c,a). Specifically, the SFR of each X-ray AGN is divided by the SFR of galaxies in the control sample that are within ±0.2 dex in M_*, ±0.075 × (1 + z) in redshift and are in similar density fields. Furthermore, each source is weighted based on the uncertainty of the SFR and M_* measurements made by CIGALE. Then, the median values of these ratios are used as the SFR_{norm} of each X-ray AGN. We note that our measurements are not sensitive to the choice of the box size around the AGN. Selecting smaller boxes, though, has an effect on the errors of the calculations (Mountrichas et al. 2021).

The top panel of Fig. 3 presents the SFR_{norm} as a function of L_X, for different cosmic environments. Measurements are the median values of SFR_{norm} grouped in bins of L_X of size 0.5 dex. The errors presented are 1σ, calculated using bootstrap resampling (e.g., Loh 2008). Only bins that have more than 10 sources are presented. We notice that the SFR_{norm}-L_X relation is flat for sources found in the field. However, an increase of SFR_{norm} is observed, in particular at $\log[L_{X,2-10keV}(\mathrm{erg\,s^{-1}})] > 43$, for sources associated with filaments and clusters. This implies that for X-ray luminosities probed by our dataset, AGN in the field have lower SFR compared to the SFR of non-AGN systems, regardless of the L_X. However, in denser environments, the SFR of AGN compared to non-AGN galaxies depends on the L_X. At $\log[L_{X,2-10keV}(\mathrm{erg\,s^{-1}})] < 43$, AGN appear to have lower SFR compared to non-AGN, wheras at moderate L_X, AGN have similar or larger SFR compared to non-AGN systems. Previous studies (Mountrichas et al. 2022c,a), found that the SFR of low to moderate L_X AGN (i.e., $\log[L_{X,2-10keV}(\mathrm{erg\,s^{-1}})] < 44$) is lower, or at most equal to the SFR of non-AGN systems. In light of our current measurements, these previous results could be attributed to the density field of the sources. That is, low to moderate L_X AGN have lower SFR compared to non-AGN systems when both populations are found in the field, but the SFR of (moderate L_X) X-ray AGN is similar or larger to that of non-AGN galaxies when the sources are associated with filaments or clusters.

We repeat the same exercise, but we now classify AGN and non-AGN using their overdensity values. Specifically, those sources that have overdensity values that belong to the highest 20% of the total samples are classified as sources in 'high density fields', whereas those with overdensity values that belong to the lowest 20% of the total samples are characterized as sources in 'low density fields'. Sources that belong to the 'high density field' group have $\log(1 + \delta) > 0.28$ (both in the case of AGN and non-AGN galaxies), whereas those in the 'low density field' group have $\log(1 + \delta) < -0.12$. The SFR_{norm} as a function of the L_X for the two classes is presented in the middle panel of Fig. 3. These results confirm our previous observations, but the trends are now more clear and appear statistical significant. Specifically, SFR_{norm} in denser fields is higher compared to fields of low density, at a ~ 2σ significance level and there is an increase of SFR_{norm} with L_X for sources in dense environments, whereas in fields of low density the SFR_{norm}-L_X relation is flat and SFR_{norm} is consistently lower than 1 (i.e., the SFR of AGN is lower compared to the SFR of non-AGN galaxies).

To examine if our results are affected by possible evolution with cosmic time within the redshift range that our datasets span ($0.3 < z < 1.2$), we restrict our samples to a narrow redshift interval, that is $0.8 \le z \le 1.2$. There are 238 AGN and 8019 sources in the control sample within this redshift range. The results using these subsets are presented in the bottom panel of Fig. 3. The statistical uncertainties are larger due to the smaller size of the subsets used, but the same trends are observed with those using the sources within the wider redshift interval.

Next, we examine if the trends observed above for the total AGN and non-AGN galaxies, hold in the case of star-forming sources, that is after excluding quiescent (Q) systems. In our previous studies (Mountrichas et al. 2021, 2022c,a), we have identified quiescent systems (both AGN and non-AGN galaxies), using their specific SFR measurements (sSFR = $\frac{SFR}{M_*}$) and we have excluded them from our analysis, when studying the SFR_{norm}-L_X relation. Therefore, we now use systems identified as quiescent in Mountrichas et al. (2022c) (see their Sect. 3.5) that studied the SFR_{norm}-L_X in the COSMOS field, and we examine whether

their fraction differs between AGN and non-AGN galaxies, in different cosmic environments. We find that the fraction of quiescent sources increases in denser fields for non-AGN galaxies, from ∼ 25% for isolated galaxies (or galaxies in low density fields) to ∼ 40% in the most dense environments. In the case of AGN, the fraction of quiescent systems is similar in all environments (∼ 30%).

We, then, repeat the SFR_{norm}-L_X measurements, excluding quiescent systems. The results are presented in Fig. 4. We note that due to the smaller size of these samples, there is only one bin that satisfies our requirement for the minimum number of sources (> 10), in the case of AGN in clusters. Overall, when quiescent systems are not included in the analysis, the amplitude of SFR_{norm} is lower (by ∼ 0.2 dex) for all cosmic environments and L_X spanned by our datasets compared to the SFR_{norm} values derived using the total samples (Fig. 3). However, the trends mentioned earlier remain unchanged. Specifically, SFR_{norm} is higher for denser environments and an increase of SFR_{norm} with L_X is observed for sources associated with filaments/clusters.

4.2. The star-formation histories of AGN and non-AGN galaxies, as a function of the cosmic environment

In this section, we study the SFH of AGN and non-AGN galaxies. Our goal is to check whether their stellar populations agree with the picture drawn in Sect. 4.1 (e.g., systems with lower SFR are expected to have older stars compared to systems with higher SFR). Moreover, the study of the SFH could allow us to reveal what drives the trends we observed in the previous section. We note that the selection of sources with available D_n4000 and H_δ measurements does not bias our samples against Q systems. In other words, the AGN and non-AGN datasets used in this part of our analysis, include the same fraction of Q systems with the datasets used in the previous section. Therefore, a direct comparison can be made of the results of these two parts of our analysis.

Fig. 5 presents the distributions of AGN and non-AGN galaxies in the H_δ-D_n4000 space, for sources in the field (top panel) and those associated with filaments (middle panel) and clusters (bottom panel). Prompted by the results in the previous section, we split our AGN into two L_X bins, at $\log[L_{X,2-10keV}(erg\,s^{-1})] = 43$. Red circles indicate AGN with $\log[L_{X,2-10keV}(erg\,s^{-1})] > 43$ ('moderate L_X') and orange circles represent AGN with $\log[L_{X,2-10keV}(erg\,s^{-1})] < 43$ ('low L_X'). The number of AGN and non-AGN available are presented in Table 1.

Regarding, the D_n4000 and H_δ distributions for AGN and non-AGN galaxies that are in the field (top panel of Fig. 5), we notice that the two AGN populations have similar stellar ages, which are higher compared to non-AGN systems. A KS test yields a p-value of ∼ 1 for the D_n4000 distributions of low and moderate L_X AGN. Comparing the distributions between AGN and non-AGN galaxies, we get a p-value of 0.20 and 0.008 for the D_n4000 distributions of moderate and low L_X AGN compared to non-AGN systems, that indicates a statistically significant difference, at least in the case of low L_X AGN compared to non-AGN. AGN, also, tend to have lower H_δ values compared to sources in the control sample. However, based on a KS test, this difference does not appear statistically significant. Merging the two AGN populations and comparing their H_δ and D_n4000 distributions with those of their non-AGN counterparts does not affect the overall results. Specifically, AGN appear to have higher D_n4000 and lower H_δ values compared to non-AGN galaxies. Based on the p-values of the KS tests, the first difference is sta-
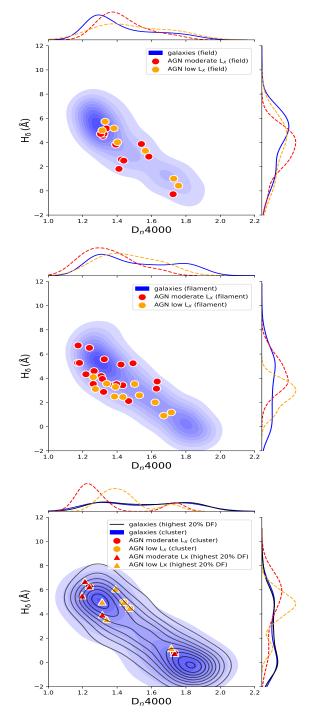

Fig. 5: The distributions in the H_δ-D_n4000 space of non-AGN galaxies (blue shaded contours) and low $(\log[L_{X,2-10keV}(erg\,s^{-1})] < 43$; orange circles) and high $(43 < \log[L_{X,2-10keV}(erg\,s^{-1})] < 44$; red circles) L_X AGN, for different cosmic environments. The top panel, presents the distribution for isolated sources (field), the middle panel for sources associated with filaments and the bottom panel for sources found in the most dense fields (see text for more details).

tistically significant (p-value of 0.02 and 0.05, respectively, for D_n4000 and H_δ).

The above suggest that AGN that live in the field tend to have older stellar populations and are less likely to have experienced a recent star-formation burst compared to isolated non-AGN sys-

tems. These results are in agreement with those presented in Fig. 3. The picture that emerges is that AGN that are in the field have similar star-formation rates and histories regardless of the AGN power (L_X) and have, on average, lower SFR and older stellar ages compared to their non-AGN field counterparts.

On the other hand, as shown in the middle panel of Fig. 5, AGN that live in denser environments (i.e., filaments) have different star-formation histories, depending on their L_X. Specifically, AGN with $\log[L_{X,2-10keV}(erg\,s^{-1})] > 43$ tend to have lower D_n4000 (= 1.32 vs. = 1.44) and higher H_δ values (= 4.20 vs. = 2.56), compared to their lower L_X counterparts (p-value of ~ 0.3, for both spectral indices). These differences, although not statistically significant based on KS tests, are in agreement with the results we found in the previous section, where higher L_X AGN have increased SFR_{norm} compared to lower L_X sources. Regarding the non-AGN galaxies, these appear to have flatter D_n4000 and H_δ distributions compared to AGN (median $D_n4000 = 1.46$, $H_\delta = 3.46$).

Finally, the bottom panel of Fig. 5, presents the D_n4000 and H_δ distributions for AGN and non-AGN systems that are associated with the most dense cosmic environments. Since there are only four AGN that live in clusters in our dataset, we also follow the same approach we followed in the previous section. That is, we also classify sources based on their overdensity values. We notice that the results are very similar, both for the D_n4000 and the H_δ, for the non-AGN galaxies, regardless of whether the classification is based on the cosmic environment (clusters) or the overdensity value (i.e., the solid black and red lines). AGN with $\log[L_{X,2-10keV}(erg\,s^{-1})] > 43$ have lower D_n4000 and higher H_δ values compared to their lower L_X counterparts (p-value of 0.00003 and 0.004, for D_n4000 and H_δ, respectively) and the non-AGN galaxies (p-value of 0.02 and 0.006, for D_n4000 and H_δ, respectively). Based on the p-values of the KS-tests, these differences are statistically significant at a level of $> 2\sigma$. This confirms our findings, presented in the previous section, for higher SFR of high L_X AGN compared to lower L_X X-ray sources and non-AGN systems.

Table 1 shows the median D_n4000 and H_δ values for the different populations and cosmic environments. Non-AGN galaxies tend to have higher D_n4000 and lower H_δ values as we move to denser fields, which indicate that their stellar population becomes older in denser environments, in agreement with most previous studies (e.g., Pérez-Millán et al. 2023). In addition to the median values presented in Table 1, there are noteworthy differences in the D_n4000 and H_δ distributions of galaxies in different cosmic environments (Fig. 5). For galaxies in the field, the two distributions, present a long tail. This tail becomes more prominent for sources associated with filaments and in the case of galaxies in the densest environments the distributions become flat. We confirm that these long tails/secondary peaks are populated, mainly, by Q galaxies and their prominence is associated with the increased fraction of Q non-AGN systems in denser environments.

On the other hand, AGN and in particular X-ray sources with $\log[L_{X,2-10keV}(erg\,s^{-1})] < 43$ have consistent H_δ and, especially, D_n4000 values in all cosmic environments (Table 1) and their D_n4000 and H_δ distributions have less prominent tails compared to non-AGN galaxies (Fig. 5). More luminous AGN show a tendency of lower D_n4000 and higher H_δ values in the most dense environments, although the sub-sample is small and larger datasets are required to confirm these findings.

These results can provide an explanation as to what drives the trends we observed in the previous section. Specifically, the increase of the SFR_{norm} as we move from the field to filaments

and to clusters (Fig. 3) is mainly driven by the lower SFR of galaxies in higher density fields and to a lesser degree due to the increased SFR of the more luminous AGN in denser cosmic environments.

We repeat the same exercise, separating now the sources into SF and Q systems. The results are shown in Table 2. Due to the small number of available AGN we do not split the AGN based on their L_X. We also characterize the cosmic environment of sources based on their overdensity values (see Sect. 4.1). The results show that the stellar populations of Q systems, both in the case of AGN and non-AGN galaxies, depend on the cosmic environment, whereas for SF systems the differences with the density field are smaller. We note, however, that in the case of AGN, the measurements come from a small number of sources in each density field. Specifically, both at high and low density fields, our AGN subsamples include eight SF and three Q systems.

4.3. Environment vs. morphology

In this section, we examine the morphology of AGN and non-AGN galaxies, in different cosmic environments. This will allow us to study the SFH of AGN and non-AGN systems in different environments, at fixed morphological type. It will also enable us to examine the link between morphology (e.g., BD) and galaxy phase (e.g., Q) for the two populations.

There are nine (24%) AGN in our dataset that live in BD systems. A similar fraction (21%) of BD galaxies is also found in the non-AGN sample. We also note that the fraction of Q systems is similar (~ 40%) for AGN and non-AGN galaxies. We find similar fractions between the AGN and the galaxies in the control sample to be associated with fields, filaments and clusters (see Table 3). A noteworthy difference, though, is that the percentage of BD systems shows an (mild) increase towards higher density environments among the non-AGN galaxies, similar to the increase of the fraction of Q systems in denser fields. On the contrary, the percentage of BD systems that also host AGN is significantly reduced in AGN associated with dense cosmic environments, while the fraction of Q AGN hosts remains roughly the same, independently of the density field. When we associate sources with high density regions based on the overdensity values of the sources, the fractions of BD systems in both the AGN and the non-AGN datasets (numbers in square brackets in Table 3) is the same as those we found using their cosmic environment, and therefore the same conclusions are reached.

Therefore, based on our analysis, BD systems are nearly equally likely to be found in non-AGN galaxies regardless of their cosmic environment. In the case of galaxies that host (type 2) AGN, BD systems are preferentially found in AGN associated with less dense fields. Moreover, the link between morphology (BD) and galaxy phase (Q) is weaker for AGN compared to non-AGN galaxies. This is confirmed by the study of the stellar populations, presented in Table 3. The stellar population of non-AGN galaxies is different for BD and non-BD systems, as opposed to galaxies that host AGN, in which case smaller differences are observed in the stellar populations for different morphologies (see also Mountrichas et al. 2022b). We note, however, that in the case of AGN the size of the available dataset is small and larger samples are required to confirm our findings.

5. Discussion

Previous galaxy studies that have examined the role of the cosmic environment and morphology on the star-formation have

Table 1: Number of X-ray AGN and sources in the control sample with available D_n4000 and H_δ measurements from the LEGA-C catalogue, in different cosmic environments. Median D_n4000 and H_δ values of each subset is also presented.

	field		filament		cluster	
L_X (erg/s)	$< 10^{43}$	$\geq 10^{43}$	$< 10^{43}$	$\geq 10^{43}$	$< 10^{43}$	$\geq 10^{43}$
no. AGN	7	11	11	19	2 (6)	2 (5)
D_n4000, H_δ (AGN)	1.40, 4.00	1.41, 3.89	1.44, 2.56	1.32, 4.20	1.44, 4.95	1.22, 5.53
no. galaxies	490		603		79 (244)	
D_n4000, H_δ (galaxies)	1.36, 4.45		1.46, 3.46		1.55, 2.23	

Notes. Numbers in the parentheses show the number of AGN when we classify sources using their overdensity values (see text for more details).

Table 2: Median D_n4000 and H_δ values for star-forming (SF) and quiescent (Q) AGN and non-AGN galaxies in different density fields.

	low density field		high density field	
	SF	Q	SF	Q
D_n4000, H_δ (AGN)	1.31, 4.18	1.44, 0.27	1.34, 4.98	1.72, 1.17
D_n4000, H_δ (galaxies)	1.30, 5.13	1.67, 1.74	1.35, 1.78	1.78, 0.21

Table 3: Number of X-ray AGN and sources in the control sample for different morphologies and cosmic environments. The median D_n4000 and H_δ values of each subset is also presented.

	field		filament		cluster	
morphology	BD	non-BD	BD	non-BD	BD	non-BD
no. AGN	12 (32%)		21 (57%)		4 (11%) [13]	
AGN	6(50%)	6(50%)	3(14%)	18(86%)	0(0%) [0(0%)]	4(100%) [13(100%)]
D_n4000, H_δ (AGN)	1.58, 5.00	1.40, 4.54	1.63, 2.58	1.42, 3.43	nan, nan	1.47, 4.98
no. galaxies	494(41%)		560(53%)		72(7%) [218]	
galaxies	87(19%)	367(81%)	121(22%)	439(78%)	20(28%) [62(28%)]	52(72%) [156(72%)]
D_n4000, H_δ (galaxies)	1.67, 1.23	1.32, 5.03	1.76, 0.64	1.38, 4.19	1.80, -0.04	1.40, 3.62

Notes. Numbers in the square brackets show the number of AGN when we classify sources using their overdensity values (see text for more details).

found controversial results. For instance, Erfanianfar et al. (2016), used X-ray-selected galaxy groups and found little dependence of the star-formation on environment at $0.5 < z < 1.1$, for main-sequence (MS) galaxies. Their findings suggest that stellar mass, morphology and environment act together in moving the star formation to lower levels. However, environmental effects are more prominent at lower redshifts. Darvish et al. (2016) used star-forming and quiescent galaxies in the COSMOS field at $z \leq 3$. They found that star-forming galaxies have similar SFR and sSFR in different environments, regardless of their redshift and M_*. The fraction of Q systems depends on the environment at $z \leq 1$ and on M_* out to $z \sim 3$. Moreover, galaxies at $z \leq 1$ become Q faster in denser environments and the overall environmental quenching efficiency increases with cosmic time. They also concluded that environmental and mass quenching processes depend on each other and they become prominent at different cosmic time. Specifically, environmental quenching is only relevant at $z \leq 1$, whereas mass quenching is the dominant mechanism at $z \geq 1$. Leslie et al. (2020) used galaxies in the COSMOS field and found no variations in the main-sequence in different environments. Albeit, they found that BD galaxies have lower SFR than disk-dominated galaxies, at fixed M_* at $z < 1.2$. Delgado et al. (2022) studied galaxy members in 80 groups at $z \leq 0.8$ and found, among others, that the fraction of red and quiescent galaxies is always higher in groups than in the field. More recently, Cooke et al. (2023), used star-forming galaxies in the COSMOS field and found no environmental and morphological dependence of the shape of the MS, up to redshift of 3.5. Pérez-Millán et al. (2023) performed a detailed study on the dependence of the observed galaxy properties on M_*, morphology and environment and found that at fixed M_* and morphology, clusters have higher quenching efficiencies. They conclude that the cluster environment affects the ability to form stars, independent of morphological type. Sobral et al. (2022) used the LEGA-C catalogue and the local overdensities estimated by Darvish et al. (2015, 2017) and found that the fraction of Q galaxies hinges on M_* and on the environmental density. Their findings also showed that the D_n4000 and H_δ indices of galaxies depends on M_* and on the cosmic environment, in particular, in the case of Q galaxies, whereas for SF systems the two spectral indices depend, mainly, on M_* and do not show a significance dependence on environment. They concluded that Q galaxies in higher density fields are older, formed and/or quenched earlier.

Our analysis shows that galaxies with $\log [M_*(M_\odot)] > 10.6$, at $z \sim 1$, have different stellar populations in different cosmic environments (Table 1) and these differences are, mainly driven by Q (or BD) systems (Table 2 and 3), in agreement with, for instance, Sobral et al. (2022). Our results, also, show that galaxy morphology is affected by the environment, with the fraction of BD systems to increase with the density field (see also e.g., Dressler 1980; Fasano et al. 2015). Recently, Hasan et al. (2023) analyzed outputs from the Illustris-TNG-100 magnetohydrody-

namical cosmological simulations ([Pillepich et al. 2018](); [Nelson et al. 2019]()). Their analysis showed that the influence of the cosmic environment on the star formation activity starts at z ∼ 2 and that most of the star formation-environment relationships can be explain in terms of the evolution of the median gas fraction. Specifically, the quenching of star formation in dense environments is due to rapid gas stripping or in the case of intermediate density fields due to gradual gas starvation.

The main aspect of this work is the role of the SMBH activity in the star formation and stellar population of galaxies in different environments (and morphologies). Our results showed that galaxies that host low luminosity AGN ($\log[L_{X,2-10keV}(\mathrm{erg\,s^{-1}})] < 43$) have, on average, consistent stellar populations independent of the cosmic environment. Their SFR is also lower compared to the SFR of non-AGN galaxies ($SFR_{norm} \sim 1$), regardless of the field density. Galaxies that host moderate L_X AGN ($43 < \log[L_{X,2-10keV}(\mathrm{erg\,s^{-1}})] < 44$) have stellar populations that tend to be younger in denser fields compared to the field. Their SFR is also similar, if not higher, compared to the SFR of non-AGN galaxies ($SFR_{norm} \geq 1$). This could imply that the AGN feedback in dense environments counter-acts the removal of the gas and prevents the quenching of the star formation (positive feedback; e.g., [Zinn et al. 2013](); [Santoro et al. 2016](); [Meenakshi et al. 2022]()). The higher the AGN activity (L_X), the most efficient the AGN feedback. However, an alternative interpretation of our results could be that a common mechanism (for instance mergers, e.g., [Di Matteo et al. 2005](); [Hopkins et al. 2008]()) feeds both the star formation and the SMBH and triggers the SF and the AGN activity (e.g., [Bower et al. 2006](); [Fanidakis et al. 2012]()). In this scenario, the more gas funnelled to the galaxy due to the triggering mechanism, the higher the increase of the SFR and the AGN power (L_X). This picture is also consistent with the different morphological types that prevail in different environments between AGN and non-AGN systems. Specifically, the rarity of BD galaxies in systems that host AGN in dense fields, could be an indication of galaxy interactions that trigger both phenomena. Finally, the lower SFR of galaxies that host AGN compared to non-AGN systems ($SFR_{norm} < 1$), in low dense fields, could be explained by low availability of gas in these systems. For instance, [Zubovas et al. (2013)]() showed that in galaxies that are in a gas-poor phase AGN feedback may quench the star formation.

6. Conclusions

We used 551 X-ray AGN and 16917 non-AGN galaxies, at $0.3 < z < 1.2$, in the COSMOS field to compare their SFR (SFR_{norm}) as a function of L_X, in different cosmic environments. We restrict the M_* of both population to the range of $10.5 < \log[M_*(M_\odot)] < 11.5$. The classification of the sources in three environments (field, filaments, clusters) is available from the catalogue of [Yang et al. (2018)](). The categorization is based on their field density using the method described in [Darvish et al. (2015)](). The (host) galaxy properties were calculated via SED fitting, using the CIGALE code and the measurements have been presented in [Mountrichas et al. (2022c)](). We then, cross-matched our datasets with the LEGA-C catalogue that allowed us to study the SFH of the two populations, for different field densities. This information is available for 52 AGN and 1172 non AGN galaxies. Finally, we compared the role of environment vs. morphology, using the morphological information in the catalogue of [Ni et al. (2021)](), using 37 AGN and 1086 non-AGN galaxies that are common between the datasets. Our main results can be summarized as follows:

- The SFR of galaxies that host AGN is lower compared to the SFR of non-AGN systems ($SFR_{norm} < 1$), for isolated sources (field), at all L_X spanned by our dataset ($42 < \log[L_{X,2-10keV}(\mathrm{erg\,s^{-1}})] < 44$). However, in denser environments an increase of SFR_{norm} ($SFR_{norm} \sim 1$) is observed at intermediate L_X ($\log[L_{X,2-10keV}(\mathrm{erg\,s^{-1}})] > 43$).
- SFR_{norm} appears higher in fields of higher density compared to lower density fields.
- Non-AGN galaxies tend to have older stellar populations (higher D_n4000 values) and are less likely to have undergone a recent star-formation burst (lower H_δ values) in denser environments compared to isolated sources (field). On the contrary, low L_X AGN have consistent stellar populations (similar D_n4000 and H_δ values), in all cosmic environments, while moderate L_X AGN tend to have younger stars and are more likely to have undergone a recent burst, in high density fields.
- The differences of the stellar populations for different cosmic environments are, mainly, driven by quiescent systems, both in the case of AGN and non-AGN galaxies.
- Although the same fraction of AGN and non-AGN systems is associated with different cosmic environments and the same fraction of BD systems is found both for AGN and non-AGN galaxies, the morphology as a function of the environment is different for the two populations. Specifically, in the case of non-AGN galaxies, the percentage of BD systems increases with the field density, whereas in the case of AGN, BD systems become scarce in denser environments.

In this work, we studied the SFR and stellar populations of AGN and non-AGN galaxies in different cosmic environments (and morphologies). Larger samples that include sources observed in wider fields, such as the eFEDS field, would be extremely useful to confirm our findings and expand our investigations to larger M_*, L_X and redshift baselines. Previous studies have showcased the importance of M_* when comparing the star formation and stellar populations of AGN and non-AGN systems. Therefore, larger samples that span, in sufficient numbers, lower ($\log[M_*(M_\odot)] < 10.5$) and higher ($\log[M_*(M_\odot)] > 11.5$) M_* are important to examine if our results change at different M_* regimes. Datasets that cover a wider redshift baseline, will also allow to examine a possible dependence with cosmic time. Finally, the X-ray AGN used in this study, probe low-to-moderate L_X. It would be particularly interesting to check if and how the results change in the case of the most powerful AGN ($\log[L_{X,2-10keV}(\mathrm{erg\,s^{-1}})] > 44$).

References

Aragón-Calvo, M. A., Jones, B. J. T., van de Weygaert, R., & van der Hulst, J. M. 2007, Astronomy & Astrophysics, 474, 315

Bernhard, E., Grimmett, L. P., Mullaney, J. R., et al. 2019, Monthly Notices of the Royal Astronomical Society: Letters, 483, L52

Boquien, M., Burgarella, D., Roehlly, Y., et al. 2019, Astronomy & Astrophysics, 622, A103

Bower, R. G., Benson, A. J., Malbon, R., et al. 2006, MNRAS, 370, 645

Boyle, B. J., Shanks, T., Croom, S. M., et al. 2000, Monthly Notices of the Royal Astronomical Society, 317, 1014

Brambila, D., Lopes, P. A. A., Ribeiro, A. L. B., & Cortesi, A. 2023, Monthly Notices of the Royal Astronomical Society

Bruzual, G. & Charlot, S. 2003, MNRAS, 344, 1000

Buat, V., Ciesla, L., Boquien, M., Małek, K., & Burgarella, D. 2019, Astronomy & Astrophysics, 632, A79

Buat, V., Mountrichas, G., Yang, G., et al. 2021, A&A, 654, A93

Charlot, S. & Fall, S. M. 2000, ApJ, 539, 718

Ciesla, L., Elbaz, D., & Fensch, J. 2017, Astronomy & Astrophysics, 608, A41

Civano, F., Marchesi, S., Comastri, A., et al. 2016, ApJ, 819, 62

Cooke, K. C., Kartaltepe, J. S., Rose, C., et al. 2023, The Astrophysical Journal, 942, 49

Dale, D. A., Helou, G., Magdis, G. E., et al. 2014, ApJ, 784, 83

Darvish, B., Mobasher, B., Martin, D. C., et al. 2017, The Astrophysical Journal, 837, 16

Darvish, B., Mobasher, B., Sobral, D., et al. 2016, The Astrophysical Journal, 825, 113

Darvish, B., Mobasher, B., Sobral, D., Scoville, N., & Aragon-Calvo, M. 2015, The Astrophysical Journal, 805, 121

Darvish, B., Sobral, D., Mobasher, B., et al. 2014, The Astrophysical Journal, 796, 51

Delgado, R. M. G., Rodriguez-Martin, J. E., Díaz-García, L. A., et al. 2022, Astronomy & Astrophysics, 666, A84

Di Matteo, T., Springel, V., & Hernquist, L. 2005, Nature, 433, 604

Dressler, A. 1980, The Astrophysical Journal, 236, 351

Elbaz, D., Daddi, E., Borgne, D. L., et al. 2007, Astronomy & Astrophysics, 468, 33

Erfanianfar, G., Popesso, P., Finoguenov, A., et al. 2016, Monthly Notices of the Royal Astronomical Society, 455, 2839

Fanidakis, N. et al. 2012, MNRAS, 419, 2797

Fasano, G., Poggianti, B. M., Bettoni, D., et al. 2015, Monthly Notices of the Royal Astronomical Society, 449, 3927

Ferrarese, L. & Merritt, D. 2000, ApJ, 539, 9

Florez, J., Jogee, S., Sherman, S., et al. 2020, Monthly Notices of the Royal Astronomical Society, 497, 3273

Hasan, F., Burchett, J. N., Abeyta, A., et al. 2023, How Cosmic Web Environment Affects Galaxy Quenching Across Cosmic Time

Hopkins, P. F., Hernquist, L., Cox, T. J., & Keres, D. 2008, ApJS, 175, 356

Inoue, A. K. 2011, Monthly Notices of the Royal Astronomical Society, 415, 2920

Kauffmann, G., Heckman, T. M., White, D. M. S., et al. 2003, Monthly Notices of the Royal Astronomical Society, 341, 33

Komatsu, E., Smith, K. M., Dunkley, J., et al. 2011, The Astrophysical Journal Supplement Series, 192, 18

Kormendy, J. & Ho, L. C. 2013, ARAA, 51, 511

Koutoulidis, L., Mountrichas, G., Georgantopoulos, I., Pouliasis, E., & Plionis, M. 2022, Astronomy & Astrophysics, 658, A35

Laigle, C., McCracken, H. J., Ilbert, O., et al. 2016, ApJS, 224, 24

Lanzuisi, G. et al. 2017, A&A, 602, 13

Leslie, S. K., Schinnerer, E., Liu, D., et al. 2020, The Astrophysical Journal, 899, 58

Lin, L., Jian, H.-Y., Foucaud, S., et al. 2014, The Astrophysical Journal, 782, 33

Loh, J. M. 2008, ApJ, 681, 726

Lutz, D. et al. 2010, ApJ, 712, 1287

Magorrian, J. et al. 1998, AJ, 115, 2285

Małek, K., Buat, V., Roehlly, Y., et al. 2018, Astronomy & Astrophysics, 620, A50

Marchesi, S., Civano, F., Elvis, M., et al. 2016, ApJ, 817, 34

Masoura, V. A., Mountrichas, G., Georgantopoulos, I., & Plionis, M. 2021, Astronomy & Astrophysics, 646, A167

Masoura, V. A., Mountrichas, G., Georgantopoulos, I., et al. 2018, A&A, 618, 31

McCracken, H. J., Milvang-Jensen, B., Dunlop, J., et al. 2012, A&A, 544, A156

Meenakshi, M., Mukherjee, D., Wagner, A. Y., et al. 2022, Monthly Notices of the Royal Astronomical Society, 511, 1622

Mountrichas, G., Buat, V., Yang, G., et al. 2021, Astronomy & Astrophysics, 653, A74

Mountrichas, G., Buat, V., Yang, G., et al. 2022a, Astronomy & Astrophysics, 663, A130

Mountrichas, G., Buat, V., Yang, G., et al. 2022b, Astronomy & Astrophysics, 667, A145

Mountrichas, G., Georgakakis, A., & Georgantopoulos, I. 2019, Monthly Notices of the Royal Astronomical Society, 483, 1374

Mountrichas, G., Masoura, V. A., Xilouris, E. M., et al. 2022c, Astronomy & Astrophysics, 661, A108

Mullaney, J. R., Alexander, D. M., Aird, J., et al. 2015, Monthly Notices of the Royal Astronomical Society: Letters, 453, L83

Nelson, D., Springel, V., Pillepich, A., et al. 2019, Computational Astrophysics and Cosmology, 6

Ni, Q., Brandt, W. N., Yang, G., et al. 2021, Monthly Notices of the Royal Astronomical Society, 500, 4989

Page, M. J. et al. 2012, nat, 485, 213

Park, T., Kashyap, V. L., Siemiginowska, A., et al. 2006, The Astrophysical Journal, 652, 610

Pérez-Millán, D., Fritz, J., González-Lópezlira, R. A., et al. 2023, Monthly Notices of the Royal Astronomical Society, 521, 1292

Pillepich, A., Springel, V., Nelson, D., et al. 2018, Monthly Notices of the Royal Astronomical Society, 473, 4077

Pouliasis, E., Mountrichas, G., Georgantopoulos, I., et al. 2022, Astronomy & Astrophysics, 667, A56

Rosario, D. J., Trakhtenbrot, B., Lutz, D., et al. 2013, Astronomy & Astrophysics, 560, A72

Santoro, F., Oonk, J. B. R., Morganti, R., Oosterloo, T. A., & Tadhunter, C. 2016, Astronomy & Astrophysics, 590, A37

Santos, J. S., Altieri, B., Tanaka, M., et al. 2014, Monthly Notices of the Royal Astronomical Society, 438, 2565

Scoville, N., Arnouts, S., Aussel, H., et al. 2013, The Astrophysical Journal Supplement Series, 206, 3

Scoville, N. et al. 2007, ApJS, 172, 1

Sobral, D., Smail, I., Best, P. N., et al. 2013, Monthly Notices of the Royal Astronomical Society, 428, 1128

Sobral, D., van der Wel, A., Bezanson, R., et al. 2022, The Astrophysical Journal, 926, 117

Song, J., Fang, G., Gu, Y., Lin, Z., & Kong, X. 2023, ApJ [2305.10677]

Stalevski, M., Fritz, J., Baes, M., Nakos, T., & Popović, L. Č. 2012, Monthly Notices of the Royal Astronomical Society, 420, 2756

Stalevski, M., Ricci, C., Ueda, Y., et al. 2016, Monthly Notices of the Royal Astronomical Society, 458, 2288

Straatman, C. M. S., van der Wel, A., Bezanson, R., et al. 2018, The Astrophysical Journal Supplement Series, 239, 27

Sutherland, W. & Saunders, W. 1992, MNRAS, 259, 413

Taylor, M. B. 2005, in Astronomical Society of the Pacific Conference Series, Vol. 347, Astronomical Data Analysis Software and Systems XIV, ed. P. Shopbell, M. Britton, & R. Ebert, 29

Tremaine, S., Gebhardt, K., Bender, R., et al. 2002, The Astrophysical Journal, 574, 740

van der Wel, A., Bezanson, R., D'Eugenio, F., et al. 2021, The Astrophysical Journal Supplement Series, 256, 44

van der Wel, A., Noeske, K., Bezanson, R., et al. 2016, The Astrophysical Journal Supplement Series, 223, 29

Wu, P.-F., van der Wel, A., Gallazzi, A., et al. 2018, The Astrophysical Journal, 855, 85

Yang, G., Boquien, M., Brandt, W. N., et al. 2022, The Astrophysical Journal, 927, 192

Yang, G., Boquien, M., Buat, V., et al. 2020, Monthly Notices of the Royal Astronomical Society, 491, 740

Yang, G., Brandt, W. N., Alexander, D. M., et al. 2019, Monthly Notices of the Royal Astronomical Society, 485, 3721

Yang, G., Brandt, W. N., Darvish, B., et al. 2018, Monthly Notices of the Royal Astronomical Society, 480, 1022

Zinn, P.-C., Middelberg, E., Norris, R. P., & Dettmar, R.-J. 2013, The Astrophysical Journal, 774, 66

Zubovas, K., Nayakshin, S., King, A., & Wilkinson, M. 2013, Monthly Notices of the Royal Astronomical Society, 433, 3079